Conf-910624--1

TITLE OF SYMPOSIUM OR TITLE OF ASTM JOURNAL: 23rd National Symposium

on Fracture Mechanics

CONF-910624--1

DE91 012072

AUTHOR'S NAME:

John G. Merkle¹

TITLE OF PAPER:

Near Crack Tip Transverse Strain Effects Estimated With A Large Strain Hollow Cylinder Analogy*

AUTHOR'S AFFILIATION

¹Research specialist, Oak Ridge National Laboratory, Oak Ridge, TN 37831

DISCLAIMER

This report was prepared as an account of work sponsored by an agency of the United States Government. Neither the United States Government nor any agency thereof, nor any of their employees, makes any warranty, express or implied, or assumes any legal liability or responsibility for the accuracy, completeness, or usefulness of any information, apparatus, product, or process disclosed, or represents that its use would not infringe privately owned rights. Reference herein to any specific commercial product, process, or service by trade name, trademark, manufacturer, or otherwise does not necessarily constitute or imply its endorsement, recommendation, or favoring by the United States Government or any agency thereof. The views and opinions of authors expressed herein do not necessarily state or reflect those of the United States Government or any agency thereof.



^{*}Research sponsored by the Office of Nuclear Regulatory Research, U.S. Nuclear Regulatory Commission under Interagency Agreement 1886–8011–9B with the U.S. Department of Energy under Contract DE-AC05–840R21400 with Martin Marietta Energy Systems, Inc.

SM

The submitted manuscript has been authored by a contractor of the U.S. Government under Contract No. DE–AC05–84OR21400. Accordingly, the U.S. Government retains a nonexclusive, royalty-free license to publish or reproduce the published form of this contribution, or allow others to do so, for U.S. Government purposes.

DISCLAIMER

This report was prepared as an account of work sponsored by an agency of the United States Government. Neither the United States Government nor any agency thereof, nor any of their employees, makes any warranty, express or implied, or assumes any legal liability or responsibility for the accuracy, completeness, or usefulness of any information, apparatus, product, or process disclosed, or represents that its use would not infringe privately owned rights. Reference herein to any specific commercial product, process, or service by trade name, trademark, manufacturer, or otherwise does not necessarily constitute or imply its endorsement, recommendation, or favoring by the United States Government or any agency thereof. The views and opinions of authors expressed herein do not necessarily state or reflect those of the United States Government or any agency thereof.

DISCLAIMER

Portions of this document may be illegible in electronic image products. Images are produced from the best available original document.

ABSTRACT: In order to study effects of constraint on fracture toughness, it is important to select the right location within the crack-tip field for investigation. It is reasonable to study the region of large strains close to the crack tip within which the microscopic separations that lead to fracture actually take place. The first step in this direction was taken in 1950 by Hill, who postulated that close to a circular notch tip the principal stress directions would be radial and circumferential, so that the plastic slip lines (maximum shear stress trajectories) would be logarithmic spirals. The resulting equation for stress normal to the notch symmetry plane, neglecting strain hardening, was identical to that for the circumferential stress near the bore of an ideally plastic thick-walled hollow cylinder under external radial tension, because the relevant geometries are identical. Hill's analysis did not consider strain hardening and did not attempt to relate the notch root radius to the remotely applied load. In 1969, Rice and Johnson developed a near crack-tip, plane strain, large-strain rigid-plastic analysis considering strain hardening and assuming an infinitely sharp initial crack tip. Shortly afterwards, Merkle, following Hill's suggestion, proposed an approximate analysis of the stresses and strains ahead of a blunted crack tip on the plane of symmetry, based on a circular blunted crack tip. The analysis amounted to a hollow cylinder analogy, including the effects of strain hardening. The original hollow cylinder analogy was based on small strain theory, and the calculated strain distributions did not agree well with the Rice and Johnson results very near the blunted crack tip. Therefore, the hollow cylinder analogy equations have been rederived, based on large strain theory, and the agreement with the Rice and Johnson results and other more recent numerical results is good. Calculations illustrate the effects of transverse strain on the principal stresses very close to a blunting crack tip and show that, theoretically, a singularity still exists at the tip of a blunting crack.

KEY WORDS: fracture mechanics, crack tip blunting, transverse strain, constraint effects, large strains

NOMENCLATURE

b, b _o	Crack tip opening, current and initial, respectively, mm
c	Radial displacement of point located at initial infinitely sharp crack tip, mm
Е	Elastic modulus, MPa
e_{z}	Engineering strain in axial direction, dimensionless
$F(\epsilon)$	Function of strain which is linear in distance from crack tip, dimensionless
h	Constraint factor, dimensionless
1	Height of ring element, mm
N	Strain hardening exponent, dimensionless
R	Original distance from crack tip, mm
r, r _i	Radial distance from coordinate origin, current and initial, respectively, mm
S	Stress parameter defined by Eq. (46), MPa
u, u _r	Radial displacement, mm
\mathtt{u}_{θ}	Circumferential displacement, mm
v	Displacement defined by Eq. (57), mm
w	Axial displacement, mm
X	Undeformed horizontal coordinate, mm
X _o	Horizontal offset of hollow cylinder analogy coordinate origin from original crack tip, mm
x, y	Deformed coordinates, mm
δ_t	Crack tip opening displacement, mm
$\varepsilon_1, \varepsilon_2, \varepsilon_3$	Principal strains, dimensionless
$\varepsilon_{\theta}, \varepsilon_{r}, \varepsilon_{z}$	Circumferential, radial and axial strains, respectively, true strain unless otherwise noted, dimensionless
ϵ_{a}	Shear strain between characteristic directions at apex of large strain region, dimensionless
$\epsilon_{ m o}$	Power law reference strain, dimensionless

$\bar{\epsilon}$	Effective plastic strain, dimensionless
ϵ_y^{tr}	True crack opening strain, dimensionless
η	Maximum shear strain, dimensionless
θ	Angle measured from the crack plane, radians
λ	Strain function defined by Eq. (6), dimensionless
ν	Poisson's Ratio, dimensionless
ρ	Blunted crack or notch root radius, mm
σ	Stress, MPa
σ_1 , σ_2 , σ_3	Principal stresses, MPa
σ_{θ_i} , σ_r , σ_z	Circumferential, radial and axial stresses, MPa
$\sigma_{\boldsymbol{Y}}$	Yield stress, MPa
σ_{o}	Power law reference stress, MPa
σ_{e}	Effective stress, MPa
$\boldsymbol{\sigma}_{m}$	Mean (hydrostatic) stress, MPa
χ	Distance from blunted crack tip, mm

• .

Introduction

Fracture mechanics is a collection of material testing and analysis procedures applied for the purpose of preventing fracture due to cracks in structures. It is recognized that yielding can and does occur near the tips of cracks, the result being lower stresses and higher strains perpendicular to the crack plane than would otherwise exist. However, yielding does not necessarily prevent the buildup of hydrostatic stresses relative to shear stresses in the crack-tip plastic zone but, in fact, can amplify this buildup. This is because of the restraint of attempted transverse contractions resulting from enforced compatibility with the adjacent regions subjected to lower stresses.

Existing fracture mechanics procedures are based on the premise that, by following prescribed methods, precracked laboratory specimens can be tested under conditions of effective maximum constraint and the results transferred conservatively to structures in terms of a material property called "fracture toughness." It has been demonstrated repeatedly that below the upper shelf, fracture toughness values measured with small laboratory specimens tend to develop increased upward scatter as specimen size decreases. In the smallest specimens, dimples are visible on the specimen surfaces at the crack ends, thus demonstrating the powerful tendency for transverse contraction to occur along a crack front. This is the inevitable consequence of the constant plastic volume condition, which is one of the physical conditions governing yielding. Realizing that cracks oriented circumferentially in a pressure vessel are subjected to a nominal transverse strain condition more severe than plane strain, it is prudent to consider the possibility that a positive out-of-plane strain condition can have an effect on toughness opposite to that of transverse contraction, namely lowering the toughness.

To study the effects of constraint on fracture toughness, it is important to select the right location within the crack-tip stress and strain field for investigation. Despite the success achieved by treating K and J as single parameters that can be conveniently determined away from the crack-tip region but still assumed to control near-crack-tip behavior, understanding constraint effects has thus far not become amenable to this approach. Thus, it seems beneficial to select as a location for study the region of large strains close to the crack tip within which the microscopic separations that

lead to fracture actually take place. This approach is not a new one. In fact, it predates linearelastic fracture mechanics. However, without a mathematical or a computational connection with global structural behavior, there is no obvious way to transfer information from laboratory specimens to structures. Nevertheless, important information about the basic physical parameters governing fracture, including the nominal stress state at the flaw location, can be developed by this approach.

The first step applicable to studying the stress and strain distributions in the plastic zone immediately bordering a blunting crack tip was taken by Hill [1] in 1950. Considering a notch with a circular tip, Hill postulated that close to the notch tip the principal stress directions would be radial and circumferential and that the plastic slip-lines (maximum shear stress trajectories) would therefore be logarithmic spirals. The resulting equation for stress normal to the notch symmetry plane, neglecting strain hardening, is

$$\sigma_{\mathbf{Y}} \left[1 + \ln \left(1 + \frac{\chi}{\rho} \right) \right], \tag{1}$$

where χ is distance from the notch tip, ρ is root radius, and σ_Y is yield stress. Equation (1) is identical to the expression for the circumferential stress near the bore of an ideally plastic thick-walled hollow cylinder under external radial tension because the relevant geometries are identical.

Hill's analysis did not consider strain hardening nor attempt to relate the notch root radius to the remotely applied load. In 1969, Rice and Johnson [2] developed a near-crack-tip, plane strain, large-strain, rigid-plastic analysis considering strain hardening and assuming an infinitely sharp initial crack. Although the geometry analyzed was approximately a field of logarithmic spirals, the boundary displacement loading based on a singular shear strain distribution did not produce a perfectly circular blunted crack tip, so the slip-lines were not exactly log spirals [3]. One strain distribution on the plane of symmetry was determined for ideally plastic conditions, and the stresses were then determined for various strain-hardening exponents by integrating the equation of

equilibrium and applying the flow rule. The strain at the apex of the slip-line field was assumed to be zero [3] and, for strain hardening, a stress singularity occurred very close to the tip of the blunting crack. Because the calculated stresses at the apex of the slip-line field were finite, but the plastic strains were assumed zero and the elastic strains neglected, a state of pure hydrostatic tension was implied at that location. This result is not physically realistic enough to use in evaluating constraint effects, but the results are easily improved by assuming a finite strain at the apex, as explained in Ref. 3.

Assuming that the conditions of stress and strain near the apex of the near-tip slip-line field are only mildly sensitive to the exact shape of the blunted crack tip, Merkle, [4] following Hill's suggestion, [1] proposed an analysis of the stresses and strains ahead of a blunted crack tip on the plane of symmetry based on a circular blunted crack tip. It was reasoned that, on the plane of symmetry, the equilibrium and strain-displacement equations should be identical to those for an axisymmetrically loaded thick-walled hollow cylinder. Actually, this is only true if $\partial u_{\theta}/\partial_{\theta} = 0$, because u_{θ} changes sign at $\theta = 0$. However, as will be discussed later, numerical calculations show that this condition is approximately satisfied close to the plane of symmetry. Consequently, the hollow-cylinder analogy has the potential for illustrating details of near-crack-tip behavior without requiring complex or expensive analytical procedures. This is especially true with regard to the effects of transverse strain, because stress analysis solutions for thick-walled hollow cylinders under conditions of generalized plane strain include explicitly the effect of ε_z . The original hollow-cylinder analogy calculations [4] were based on small strain theory and therefore gave strain distributions that did not agree well with the Rice and Johnson results near the blunted crack tip. However, the original hollow-cylinder analogy did include the elastic strains, which the Rice and Johnson analysis neglected, and these strains may turn out to be important, especially the transverse (out-of-plane) elastic strain near the point of peak stress.

Basis For The Hollow-Cylinder Analogy

The basis for the hollow-cylinder analogy is Hill's approximation [1] that immediately ahead of a round-tipped notch, the slip-lines are orthogonal logarithmic spirals. Because these lines cross every radial and circumferential line at 45°, the principal directions of stress (and implicitly also of strain) are radial and circumferential, just as they are in an axisymmetrically loaded thick-walled hollow cylinder. The basic concept is thus illustrated in Fig. 1, showing that within the overall plastic zone there is a much smaller flame-shaped zone immediately ahead of the blunting crack tip within which the slip-lines are approximately logarithmic spirals. Hill's model of the region immediately ahead of a circular notch tip did not consider strain hardening, and thus nothing was said explicitly about strains. Merkle [4] extended Hill's hypothesis to include strain hardening, reasoning that stress analysis solutions for axisymmetrically loaded thick-walled hollow cylinders should be applicable on the plane of symmetry ahead of a blunting crack tip as long as the throughthickness stress remains the intermediate principal stress. Using cylindrical coordinates and recognizing that the principal directions of stress and strain in the logarithmic spiral slip-line region are radial and circumferential, it follows that all the equilibrium and conventional straindisplacement equations reduce to those for an axisymmetrically loaded thick-walled hollow cylinder except the circumferential strain-displacement equation, which for small strains is

$$\varepsilon_{\theta} = \frac{1}{r} \frac{\partial u_{\theta}}{\partial_{\theta}} + \frac{u_{r}}{r} . \tag{2}$$

For the hollow cylinder analogy to hold, $\partial u_{\theta}/\partial_{\theta}$ must be shown to be negligible or zero on the plane of symmetry. In Ref. 4, symmetry was used as an argument for setting $\partial u_{\theta}/\partial_{\theta} = 0$ on $\theta = 0^{\circ}$. However, because u_{θ} changes sign while passing through zero at $\theta = 0^{\circ}$, $\partial u_{\theta}/\partial_{\theta}$ theoretically does not have to be zero on the plane of symmetry. Thus, additional information must be used to determine if $\partial u_{\theta}/\partial_{\theta}$ is actually small enough to neglect on the plane of symmetry.

Two separate studies of the stresses and strains very close to a blunting crack tip by the finiteelement method have produced results that support the hollow-cylinder analogy. As indicated in Fig. 2, McMeeking [5] performed near-crack-tip, elastic-plastic large-strain calculations showing that the variation of effective plastic strain with polar angle θ near the plane of symmetry is very small. Needleman and Tvergaard [6] performed similar calculations, observing the details of deformation immediately surrounding the blunting crack tip. Figure 3 shows the existence of a wedge of finite elements bisected by the plane of symmetry that continues to subtend the same 22° angle as deformation proceeds. Together, Figs. 2 and 3 imply that, within a finite angular sector ahead of a blunting crack tip, material points displace only in the radial direction and circular arcs remain approximately circular. Consequently, within a finite angular sector ahead of a blunting crack tip, $u_{\theta} = 0$. For these conditions, Eq. (2) reduces to

$$\varepsilon_{\theta} = \frac{u_{r}}{r},\tag{3}$$

thus providing an empirical basis for the hollow-cylinder analogy.

Derivation of Strain-Displacement Equations For Large Strains

The original hollow-cylinder analogy [4] was developed using the conventional small-strain, elastic-plastic stress and strain equations for a thick-walled hollow cylinder. However, comparing the calculated near-crack-tip strain distribution with the results obtained by Rice and Johnson [2] showed a discrepancy, the most likely cause of which appeared to be the existence of large strains very close to the blunted crack tip. The Rice and Johnson analysis [2] was based on large strain theory, so a large strain version of the hollow-cylinder analogy is necessary for a valid comparison between the two analytical models.

Consider a ring element within a thick-walled hollow cylinder with original inside radius r_i , thickness dr_i , and height ℓ . Let the radial displacements corresponding to r_i and $r_i + dr_i$ be u and u + du, and the uniform increase in height of the ring element be w. Neglecting elastic strains, the volume of the ring must remain constant. Thus

$$2\pi \, r_i \, dr_i \, \ell = (2\pi)(r_i + u)(dr_i + du)(\ell + w) \quad . \tag{4}$$

Define

$$e_z = \frac{W}{\ell},\tag{5}$$

and

$$\lambda = \frac{e_z}{1 + e_z} \tag{6}$$

Then

$$d(r_i u) + u du + \lambda r_i dr_i = 0 , \qquad (7)$$

so that

$$u^2 + 2r_1u - (c^2 - \lambda r_1^2) = 0$$
, (8)

where c^2 is a constant of integration. From Eq. (8), it follows that

$$u = \sqrt{(1 - \lambda)r_i^2 + c^2} - r_i$$
 (9)

Setting $r_i = 0$ gives u = c, so c is the radial displacement of a point originally located at $r_i = 0$. In terms of the CTOD,

$$c = \frac{\delta_t}{2} \tag{10}$$

For large strains, the circumferential strain is defined by

$$\varepsilon_{\theta} = \ln\left(1 + \frac{\mathbf{u}}{\mathbf{r}_{i}}\right),\tag{11}$$

so that, using Eq. (9),

$$\varepsilon_{\theta} = \frac{1}{2} \ln \left[(1 - \lambda) + \frac{c^2}{r_i^2} \right]. \tag{12}$$

Note that a singularity in strain occurs for $r_i = 0$. For large strains, the axial strain is defined by

$$\varepsilon_{\mathbf{Z}} = \ln \left(1 + \mathbf{e}_{\mathbf{Z}} \right) , \tag{13}$$

so that, from Eq. (6),

$$\varepsilon_{\mathbf{Z}} = -\ln(1 - \lambda) \quad . \tag{14}$$

For large strains, the radial strain is defined by

$$\varepsilon_{r} = \ln \left(1 + \frac{\mathrm{d}u}{\mathrm{d}r_{i}} \right) \tag{15}$$

so that, by using Eqs. (9) and (14),

$$\varepsilon_{\rm r} = -\frac{1}{2} \ln \left[(1 - \lambda) + \frac{c^2}{r_{\rm i}^2} \right] - e_{\rm z} \tag{16}$$

The foregoing equations agree with those published by McGregor, Coffin, and Fisher [7] in 1948.

For applications, it is useful to have the strain-displacement equations also expressed in terms of the deformed radius r defined by

$$\mathbf{r} = \mathbf{r_i} + \mathbf{u} \quad . \tag{17}$$

Combining Eqs. (17) and (9) gives

$$r_i^2 = \frac{r^2 - c^2}{1 - \lambda} \tag{18}$$

and by using Eq. (14),

$$r_i^2 = (r^2 - c^2)e^{\epsilon_z}$$
 (19)

From Eqs. (11) and (17), it follows that

$$\varepsilon_{\theta} = \ln \left(\frac{r}{r_i} \right), \tag{20}$$

so that, by using Eqs. (19) and (20),

$$\varepsilon_{\theta} = -\frac{1}{2} \ln \left(1 - \frac{c^2}{r^2} \right) - \frac{\varepsilon_z}{2} \ . \tag{21}$$

In Eq. (21), ε_{θ} becomes singular at r = c. By substituting Eq. (18) into Eq. (16) and using Eq. (14),

$$\varepsilon_{\rm r} = \frac{1}{2} \ln \left(1 - \frac{c^2}{r^2} \right) - \frac{\varepsilon_{\rm z}}{2} \ . \tag{22}$$

Note that the above strain-displacement equations do not include the elastic strains, which are assumed small, and also that their algebraic forms are independent of the shape of the stress-strain curve. This observation agrees with the finite-difference results obtained by Rice and Johnson [2] wherein, for plane strain, the same near-tip strain distribution was found to exist independent of the yield strain and the strain-hardening exponent.

The form of Eqs. (21) and (22) can be examined by using Mohr's Circle of Strain. For generalized plane strain and constant plastic volume, if the maximum shear strain is denoted by η and

$$\varepsilon_2 = \varepsilon_7$$
 , (23)

then ε_1 and ε_3 must be given by

$$\varepsilon_1 = \eta - \frac{\varepsilon_z}{2} \tag{24}$$

and

$$\varepsilon_3 = -\eta - \frac{\varepsilon_z}{2} \tag{25}$$

Comparisons With Numerical Calculations

Because the basis for the hollow-cylinder analogy is partly empirical and direct experimental verification is not possible, it is important to establish its accuracy by means of comparisons with other independently performed analyses. The quantity of most interest is the maximum principal tensile strain ε_{θ} acting normal to the plane of symmetry. Because the near-crack-tip strain distribution is highly nonlinear, it is convenient to construct a function of ε_{θ} that is linear with distance from the crack tip. This is possible because there is only one term containing r_i in Eq. (12). Thus, by rearranging Eq. (12), for plane strain,

$$\frac{1}{\sqrt{e^{2\varepsilon_{\theta}}-1}} = \frac{r_{i}}{c} = F(\varepsilon_{\theta}) . \tag{26}$$

Figure 4 shows the near-crack-tip strain distribution for $\theta = 0^{\circ}$ based on undeformed positions X for small-scale yielding and fully plastic conditions, as calculated by Rice and Johnson [2] using the finite-difference method. Figure 4 also shows the plots of $F(\varepsilon_v^{tr})$, constructed for each case by scaling values from the strain curves and calculating $F(\varepsilon_v^{tr})$. Substantial linearity is observed. An added advantage of the linear plot is that no distance origin has to be assumed. While Fig. 4 shows that the calculated values of $F(\varepsilon_v^{tr})$ plot close to a straight line, the distance origin is not at the original crack tip, but slightly ahead of it. This is qualitatively confirmed by Fig. 5 from Rice and Johnson, [2] which shows that the curved portion of the blunted crack profile meets a horizontal segment of the crack profile slightly ahead of the original crack tip. Thus, in this case, the coordinate origin of the approximately logarithmic spiral slip-line region lies ahead of the original crack tip. A second comparison is shown in Fig. 6 using the effective plastic strain values for $\theta = 0^{\circ}$ from Fig. 2 as calculated by McMeeking [5] using the finite-element method. Again $F(\varepsilon_{\theta})$ is nearly linear over a substantial range of R/b, where R is original distance from the crack tip and b is CTOD. Again, the curve intercept is slightly ahead of the original crack tip. Thus, two near-crack-tip analyses, the first being Rice's and Johnson's finite-difference analysis [2] and the second being McMeeking's finite-element analysis, [4] have both produced near-crack-tip strain distributions having forms close to that predicted by the hollow-cylinder analogy based on large strains.

Two other available strain distributions, calculated by the finite-element method by Needleman and Tvergaard [6] and by Goldthorpe, [8] produce plots of $F(\varepsilon_{\theta})$ (not shown) that are linear until very close to X=0 but then seem to approach a finite value of strain at X=0. Both the latter analyses were begun with finite initial notch radii, as were McMeeking's, so the reason for the difference in result is not obvious. Because both Rice and Johnson [2] and McMeeking [5] clearly recognized and demonstrated the existence of a strain singularity for sharp cracks, preference is given here to their results because they are believed to be more accurate very close to the blunting crack tip.

Because a real material cannot stand infinite strain and the blunting crack surface is free of normal stress, and therefore under low triaxial constraint, shear fracture should tend to occur very close to the blunting crack tip. This is a possible explanation for the occurrence of stretch zones.

An additional comparison can be made between the strain distributions calculated by the Rice and Johnson slip-line analysis method and the hollow-cylinder analogy discussed in this chapter. In Ref. 3, two modifications were made to the Rice and Johnson slip-line analysis method to make it more useful and more realistic. The analysis was rederived for generalized plane strain, and the maximum principal tensile strain at the apex of the slip-line field was made nonzero. It is easily shown that for a nearly plane strain degree of constraint and v = 0.3, the elastically calculated maximum principal tensile strain at a distance of two times the CTOD from the crack tip is ~1%. Thus, the total tensile strain at this location must equal or exceed this value. Assuming a total shear strain at the apex of 1%, the comparison between the modified slip-line analysis method results of Ref. 3 and the hollow-cylinder analogy results are as shown in Fig. 7. Overall, the hollowcylinder analogy is a good approximation. The assumed horizontal offset X_o for the hollowcylinder analogy governs the accuracy of the strain approximation near the blunting crack tip but has no effect near the apex of the log spiral slip-line zone. The closeness of the hollow-cylinder approximation near the apex of the slip-line zone depends on the assumed value of the shear strain at that location in the modified slip-line analysis model. Because the hollow-cylinder analogy provides a satisfactory strain estimate, the next step is to calculate the stresses on the plane of symmetry.

Stress Calculations

For radial and circumferential principal stress directions, the equation of radial equilibrium, written in terms of current radii, has the familiar form

$$\frac{d\sigma_{r}}{dr} = \frac{\sigma_{\theta} - \sigma_{r}}{r} \tag{27}$$

In this analysis the elastic strains are neglected. Thus, the usual superscript "p" on strain symbols indicating plastic strain is not used. The general equation for the Von Mises effective plastic strain is

$$\overline{\varepsilon} = \frac{\sqrt{2}}{3} \sqrt{(\varepsilon_1 - \varepsilon_2)^2 + (\varepsilon_2 - \varepsilon_3)^2 + (\varepsilon_3 - \varepsilon_1)^2}$$
(28)

Using Eqs. (21) through (25),

$$\eta = \varepsilon_{\theta} + \frac{\varepsilon_{z}}{2} \tag{29}$$

and

$$\bar{\varepsilon} = \frac{2}{\sqrt{3}} \eta \sqrt{1 + \frac{3}{4} \left(\frac{\varepsilon_z}{\eta}\right)^2} \tag{30}$$

Eliminating η from Eq. (30) gives

$$\bar{\varepsilon} = \frac{2}{\sqrt{3}} \varepsilon_{\theta} \sqrt{1 + \frac{\varepsilon_{z}}{\varepsilon_{\theta}} + \left(\frac{\varepsilon_{z}}{\varepsilon_{\theta}}\right)^{2}} \qquad (31)$$

The general equation for the Von Mises effective stress is

$$\sigma_{e} = \frac{1}{\sqrt{2}} \sqrt{(\sigma_{1} - \sigma_{2})^{2} + (\sigma_{2} - \sigma_{3})^{2} + (\sigma_{3} - \sigma_{1})^{2}} . \tag{32}$$

For deformation theory, the principal plastic strains are given by the flow rule, which can be written in the form

$$\varepsilon_{i} = \frac{1}{2} \frac{\bar{\varepsilon}}{\sigma_{e}} \frac{\partial \sigma_{e}^{2}}{\partial \sigma_{i}} . \tag{33}$$

Using Eqs. (32) and (33),

$$\left(\sigma_{\theta} - \sigma_{r}\right) = \frac{2}{\sqrt{3}}\sigma_{e}\sqrt{1 - \left(\frac{\varepsilon_{z}}{\bar{\varepsilon}}\right)^{2}}, \qquad (34)$$

as found by McGregor et al [7]. From Eq. (31),

$$\left(\frac{\varepsilon_{z}}{\overline{\varepsilon}}\right)^{2} = \frac{\frac{3}{4} \left(\frac{\varepsilon_{z}}{\varepsilon_{\theta}}\right)^{2}}{1 + \frac{\varepsilon_{z}}{\varepsilon_{\theta}} + \left(\frac{\varepsilon_{z}}{\varepsilon_{\theta}}\right)^{2}},$$
(35)

so that substituting Eq. (35) into Eq. (34) gives

$$(\sigma_{\theta} - \sigma_{r}) = \frac{2}{\sqrt{3}} \sigma_{\theta} \sqrt{\frac{1 + \frac{\varepsilon_{z}}{\varepsilon_{\theta}} + \frac{1}{4} \left(\frac{\varepsilon_{z}}{\varepsilon_{\theta}}\right)^{2}}{1 + \frac{\varepsilon_{z}}{\varepsilon_{\theta}} + \left(\frac{\varepsilon_{z}}{\varepsilon_{\theta}}\right)^{2}}}.$$
(36)

From Eq. (27),

$$d\sigma_{r} = (\sigma_{\theta} - \sigma_{r}) \frac{dr}{r}$$
(37)

Therefore, the radial stress can be calculated incrementally, starting at the free surface of the blunted crack tip and using Eq. (36) and the effective stress-strain relation, which is general. In this analysis, the effective stress-strain relation is assumed to be a pure power law, according to which

$$\sigma_{e} = \sigma_{o} \left(\frac{\bar{\varepsilon}}{\varepsilon_{o}} \right)^{N} . \tag{38}$$

Thus, substituting Eq. (31) into Eq. (38), the result into Eq. (36), and then using Eq. (37) gives

$$\frac{d\sigma_{r}}{\sigma_{o}} = \frac{2}{\sqrt{3}} \left(\frac{2}{\sqrt{3} \, \varepsilon_{\theta}} \right)^{N} \left\{ \varepsilon_{\theta}^{N} \frac{\left[1 + \frac{\varepsilon_{z}}{\varepsilon_{\theta}} + \frac{1}{4} \left(\frac{\varepsilon_{z}}{\varepsilon_{\theta}} \right)^{2} \right]^{\frac{1}{2}}}{\left[1 + \frac{\varepsilon_{z}}{\varepsilon_{\theta}} + \left(\frac{\varepsilon_{z}}{\varepsilon_{\theta}} \right)^{2} \right]^{\frac{1-N}{2}}} \right\} \frac{dr}{r} .$$
(39)

Also, by again using Eq. (37),

$$\frac{\sigma_{\theta}}{\sigma_{o}} = \frac{\sigma_{r}}{\sigma_{o}} + \frac{2}{\sqrt{3}} \left(\frac{2}{\sqrt{3} \, \varepsilon_{\theta}} \right)^{N} \left\{ \varepsilon_{\theta}^{N} \frac{\left[1 + \frac{\varepsilon_{z}}{\varepsilon_{\theta}} + \frac{1}{4} \left(\frac{\varepsilon_{z}}{\varepsilon_{\theta}} \right)^{2} \right]^{\frac{1}{2}}}{\left[1 + \frac{\varepsilon_{z}}{\varepsilon_{\theta}} + \left(\frac{\varepsilon_{z}}{\varepsilon_{\theta}} \right)^{2} \right]^{\frac{1-N}{2}}} \right\}.$$
(40)

The stresses are calculated for the deformed radii. For calculating $d\sigma_r$ from Eq. (39), the strain at the average radius over an increment of distance is used. For calculating σ_{θ} from Eq. (40), the strain at the point of interest is used.

An equation for the transverse stress σ_z can be obtained by using the flow rule, Eq. (33), and the effective stress-strain relation. The result is

$$\frac{\sigma_{z}}{\sigma_{o}} = \left(\frac{\bar{\varepsilon}}{\varepsilon_{o}}\right)^{N} \left(\frac{\varepsilon_{z}}{\bar{\varepsilon}}\right) + \frac{1}{2} \left(\frac{\sigma_{r}}{\sigma_{o}} + \frac{\sigma_{\theta}}{\sigma_{o}}\right). \tag{41}$$

A constraint factor [9] h, defined by

$$h = \frac{\sigma_m}{\sigma_e} , \qquad (42)$$

where σ_m is the hydrostatic stress, is sometimes used for comparing the severity of different stress states with regard to the possibility of fracture. The quantity h can be calculated from

$$h = \frac{1}{3} \left(\frac{\varepsilon_z}{\bar{\varepsilon}} \right) + \frac{1}{2} \frac{\left(\frac{\sigma_z}{\sigma_o} + \frac{\sigma_\theta}{\sigma_o} \right)}{\left(\frac{\bar{\varepsilon}}{\varepsilon_o} \right)^N}$$
 (43)

Effects of The Strain Singularity

The strain singularity that exists at the surface of the blunting crack tip, in the case of an infinitely sharp initial crack, has an effect on the stresses for strain-hardening material. The effect

is to cause a singularity in the crack-opening stress, which in turn can cause a minimum to occur in that stress as a function of r, as the effects of the singularity decrease and the effects of triaxial constraint begin to dominate. Because the in-plane strains are large compared with the out-of-plane strain very close to the blunting crack tip, an analysis of the effects of the singularity for the case of plane strain should be adequately descriptive.

Solving the equation of radial equilibrium, Eq. (27), for σ_{θ} and differentiating gives

$$\frac{d\sigma_{\theta}}{dr} = 2\frac{d\sigma_{r}}{dr} + r\frac{d\left(\frac{d\sigma_{r}}{dr}\right)}{dr} . \tag{44}$$

For plane strain, Eq. (39) gives

$$\frac{d\sigma_{r}}{dr} = \frac{2}{\sqrt{3}} \frac{\sigma_{o}}{r} \left(\frac{2}{\sqrt{3} \, \varepsilon_{o}} \right)^{N} \varepsilon_{\theta}^{N} \quad . \tag{45}$$

Let

$$S = \frac{2}{\sqrt{3}} \sigma_o \left(\frac{2}{\sqrt{3} \varepsilon_o} \right)^N . \tag{46}$$

Then substituting Eq. (46) into Eq. (45) gives

$$\frac{d\sigma_{r}}{dr} = \frac{S}{r} \varepsilon_{\theta}^{N} , \qquad (47)$$

and substituting Eq. (47) into Eq. (44) leads to

$$\frac{d\sigma_{\theta}}{dr} = \frac{S\epsilon_{\theta}^{N}}{r} + SN\epsilon_{\theta}^{N-1}\frac{d\epsilon_{\theta}}{dr} . \tag{48}$$

For $d\sigma_{\theta}/dr = 0$, either $\varepsilon_{\theta} = 0$ or

$$\frac{\mathrm{d}\ln\varepsilon_{\theta}}{\mathrm{d}\ln r} = -\frac{1}{N} \ . \tag{49}$$

Thus, stationary values of σ_{θ} occur at infinity and when Eq. (49) is satisfied. If there are two stationary points and the curve of σ_{θ} is positive singular at r=c, then the first stationary point must be a local minimum because a local maximum would require three stationary values between r=c and $r=\infty$. It is also possible to show that the first stationary value is a local minimum by

using Eqs. (48) and (49) to develop the expression for $d^2\sigma_\theta/d(\ln r)^2$ at the first stationary point. The result is

$$\frac{\mathrm{d}^2 \sigma_{\theta}}{\mathrm{d} (\ln r)^2} = \mathrm{NS} \, \varepsilon_{\theta}^{\mathrm{N}} \, \frac{\mathrm{d}^2 \ln \varepsilon_{\theta}}{\mathrm{d} (\ln r)^2} \,, \tag{50}$$

which gives a positive quantity.

For plane strain, the location of the local minimum can be calculated by applying Eq. (49) to Eq. (21), which gives

$$\varepsilon_{\theta} = \frac{N}{\left(\frac{r}{c}\right)^2 - 1} \ . \tag{51}$$

Using Eq. (19) for plane strain,

$$\left(\frac{\mathbf{r}}{\mathbf{c}}\right)^2 - 1 = \left(\frac{\mathbf{r}_i}{\mathbf{c}}\right)^2 , \tag{52}$$

so that substituting Eqs. (21) and (52) into Eq. (51) gives

$$\frac{\ln\left[1+\left(\frac{c}{r_i}\right)^2\right]}{\left(\frac{c}{r_i}\right)^2} = 2N .$$
 (53)

The limit of the left side of Eq. (53) as (c/r_i) approaches zero is unity. Thus, there is no local minimum for values of N exceedings 0.5. Equation (53) is plotted in Fig. 8, from which locations of the local minimum can be determined graphically.

Calculating the first increment of the radial stress very close to the blunting crack tip requires an approximation because of the singularity in the circumferential strain. For plane strain, Eq. (39) reduces to

$$\frac{d\sigma_{r}}{\sigma_{o}} = \frac{2}{\sqrt{3}} \left(\frac{2}{\sqrt{3} \, \varepsilon_{o}} \right)^{N} \varepsilon_{\theta}^{N} \frac{dr}{r} . \tag{54}$$

Also, for plane strain, Eq. (21) can be written in the form

$$\varepsilon_{\theta} = -\frac{1}{2} \ln \left[\left(1 + \frac{c}{r} \right) \left(1 - \frac{c}{r} \right) \right]. \tag{55}$$

Near the singularity, $r \sim c$ so that

$$\varepsilon_{\theta} \sim -\frac{1}{2} \ln \left[\frac{2}{c} \left(r - c \right) \right] \tag{56}$$

Let

$$\mathbf{r} - \mathbf{c} = \mathbf{v} \,. \tag{57}$$

Then noting that

$$\frac{\mathrm{dr}}{\mathrm{r}} = \frac{1}{2} \, \mathrm{d} \left(2 \frac{\mathrm{v}}{\mathrm{c}} \right) \,, \tag{58}$$

substituting Eq. (57) into Eq. (56) and the result, plus Eq. (58) into Eq. (54), gives

$$d\left(\frac{\sigma_{r}}{\sigma_{o}}\right) = \frac{\left(\ln\frac{1}{2\frac{v}{c}}\right)^{N}}{3^{(1+N)/2} \varepsilon_{o}^{N}} \left(2\frac{v}{c}\right). \tag{59}$$

Integrating by parts, neglecting the second term as small, and using Eq. (57) gives, for the first increment of radial stress,

$$\frac{\sigma_{r}}{\sigma_{o}} = \frac{2\left(\frac{r}{c} - 1\right) \left[\ln \frac{1}{2\left(\frac{r}{c} - 1\right)}\right]^{N}}{3^{(1+N)/2} \varepsilon_{o}^{N}} \left(2\frac{v}{c}\right).$$
(60)

Effects Of Transverse Strain

The foregoing equations were used to calculate the in-plane and transverse stresses for three example problems. The example problems were identical except for the values of transverse plastic strain, which were -1, 0, and +1%, respectively. The other parameters used were

 ε_0 = 0.0025, N = 0.2, and c = 0.5 δ_t . The results are plotted in Fig. 9, which shows that the effect of a given amount of transverse plastic strain of either algebraic sign is to reduce the circumferential stress from its plane strain value by the same relatively small amount. The same is true for the radial stress. This result was not anticipated because the elastic-plastic, small-strain, hollow-cylinder analogy equations [4] implied that positive transverse strain would increase the inplane stresses and that negative transverse strain would do the opposite. Nevertheless, on hindsight it is clear that the results obtained here are a direct consequence of Eqs. (21), (29), (30), (34), and (37), because, from Eqs. (21) and (29), η is independent of ε_z , only the square of ε_z appears in Eqs. (30) and (34), and ε_z does not appear in Eq. (37). Furthermore, the present results agree qualitatively with the more exact results obtained in Ref. 3. In the case of the transverse stress, also plotted in Fig. 9, positive transverse strain increases the transverse stress, and negative transverse strain does the opposite. Furthermore, the transverse stress is more affected by the transverse strain than are the in-plane stresses. The effect of increasing transverse strain is to increase the constraint factor h because of the increase in transverse stress, thereby potentially decreasing the fracture toughness.

Discussion

In comparing analyses, those presented here and in Ref. 3 neglect elastic strains, therefore assuming that all the transverse strains are plastic strains. In contrast, the small-strain, hollow-cylinder analogy equations from Ref. 4 were based on the Tresca yield criterion, which predicts no plastic strain in the direction of the intermediate principal stress, thus forcing the total strain in that direction to be completely elastic. It appears that transverse elastic and plastic strains may have opposite effects on the in-plane stresses, and therefore including the elastic strains in a near-tip analysis would be beneficial. It has also been estimated recently [10] that somewhat beyond the near-crack-tip, large-strain region, positive and negative total transverse strains do not necessarily have either opposite or identical effects because the total strains are partitioned differently into elastic and plastic parts in the two cases. Despite their approximations, the analyses developed

here and in Ref. 3 have provided valuable new information about near-crack-tip stresses and strains, especially about their magnitudes at both ends of the large strain region and the effects of transverse strain, and further developments appear feasible.

Conclusions

Large strain finite element analyses have shown that a wedge shaped zone ahead of a blunting crack tip deforms like a cylinder. Therefore, a hollow cylinder stress analysis analogy is valid in this region. Applications of this analogy based on large strain theory have produced results in good agreement with those of Rice and Johnson, and McMeeking. Furthermore, they reveal that the stresses in the large strain region ahead of a blunting crack tip are only mildly sensitive to transverse constraint, if elastic strains are neglected. Therefore, constraint effects on fracture toughness are likely to be caused by some combination of elastic strain effects in the large strain region and constraint induced stress variations just beyond the large strain region.

References

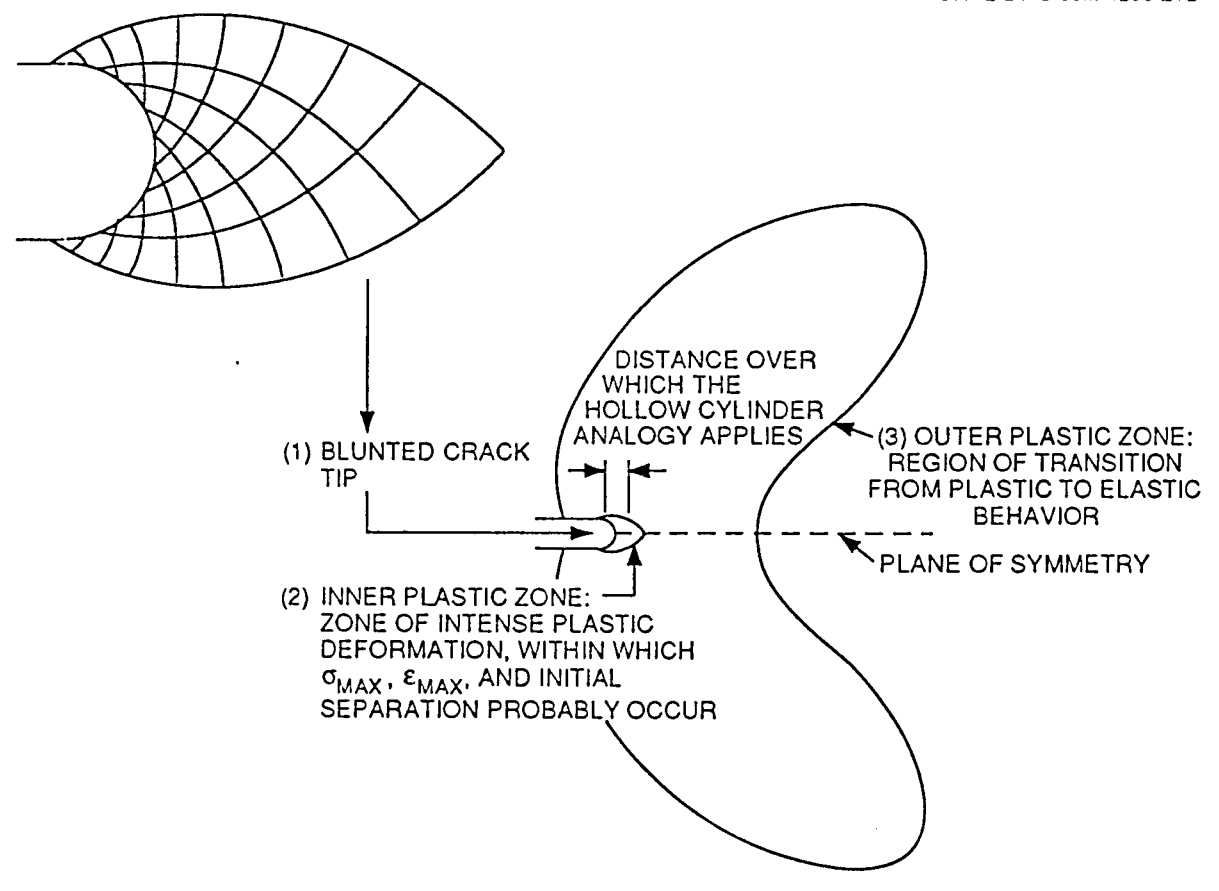
- [1] R. Hill, "The Mathematical Theory of Plasticity," Oxford Press, 1950.
- [2] J. R. Rice and M. A. Johnson, Brown University, Providence, R.I., "The Role of Large Crack Tip Geometry Changes in Plane Strain Fracture," Report NYO-2394-38, September 1969. (See also "Inelastic Behavior of Solids," M. F. Kanninen et al., eds., McGraw-Hill, 1970.)
- [3] D.K.M. Shum, "Crack Initiation Under Generalized Plane-Strain Conditions" 23rd National Symposium on Fracture Mechanics, June 18–20, 1991, College Station, Texas.
- [4] J. G. Merkle, "An Elastic-Plastic Thick-Walled Hollow Cylinder Analogy for Analyzing the Strains in the Plastic Zone Just Ahead of a Notch Tip," ORNL-TM-4071, Oak Ridge National Laboratory, Oak Ridge, Tenn., January 1973.
- [5] R. M. McMeeking, "Finite Deformation Analysis of Crack-Tip Opening in Elastic-Plastic Materials and Implications for Fracture," <u>J. Mech. Phys. Solids</u> 25, 357–381, 1977.
- [6] A. Needleman and V. Tvergaard, "Crack-Tip Stress and Deformation Fields in a Solid with a Vertex on Its Yield Surface," ASTM STP 803, I, 80–115, 1983.
- [7] C. W. MacGregor, L. F. Coffin, and J. C. Fisher, "The Plastic Flow of Thick-Walled Tubes with Large Strains," J. Appl. Phys. 19, 291–297, March 1946.
- [8] M. R. Goldthorpe, "An Investigation of Size Effects in Compact Tension and Centre-Cracked Tension Specimens of an Austenitic Steel Using Elastic-Plastic Finite Element Analysis," Report under SERC Grant No. GR/E/79088, Structural Integrity Research Institute, University of Sheffield, April 1989.
- [9] H. Kordische, E. Sommer, and W. Schmidt, "The Influence of Triaxiality on Stable Crack Growth," Nucl. Eng. Des. 112, 27–35, 1989.

[10] D. K. M. Shum, J. G. Merkle, J. Keeney-Walker, and B. R. Bass, "Analytical Studies of Transverse Strain Effects on Fracture Toughness for Circumferentially Oriented Cracks," NUREG/CR-5592 (ORNL/TM-11581), Oak Ridge National Laboratory, Oak Ridge, Tenn. (In press).

Figure Captions

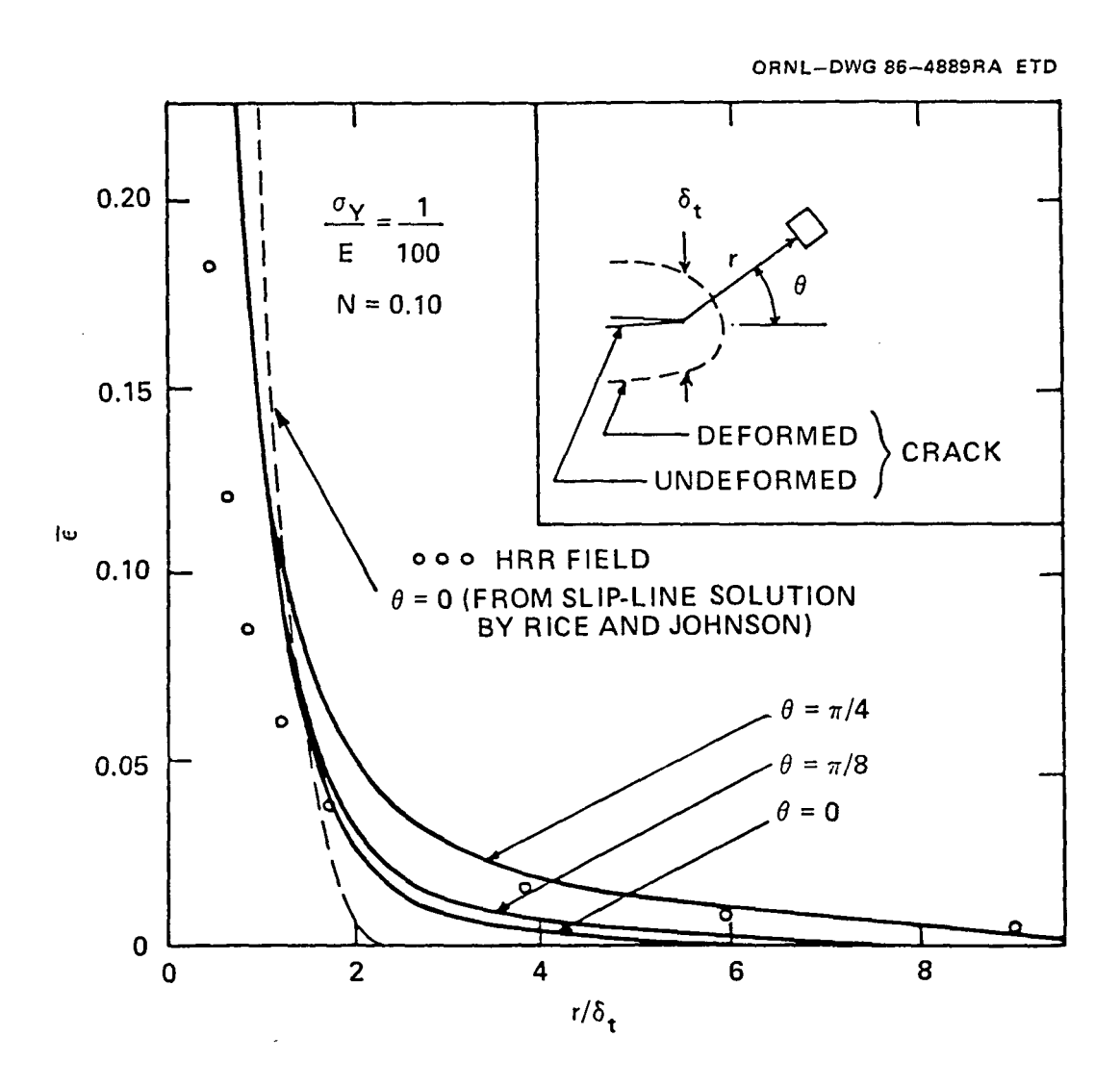
- FIG. 1--Schematic diagram of plastic zones near tip of blunting crack (Source: Ref. 4).
- FIG. 2--Effective plastic strain near a blunting crack tip (Source: Ref. 5).
- FIG. 3--Deformed finite-element mesh diagrams for blunting crack tip (based on Ref. 6).
- FIG. 4--Near-crack-tip strain and linearized strain function plots for finite-difference analysis results of Rice and Johnson (based on Ref. 2).
- FIG. 5--Deformed crack-tip and slip-line zone boundary results obtained by Rice and Johnson (Source: Ref. 2).
- FIG. 6--Linearized strain function plot for finite-element analysis results of McMeeking (based on Ref. 5).
- FIG. 7--Comparison of near-crack-tip strain distribution curves obtained by Rice and Johnson method, as described in Ref. 3, assuming $\varepsilon_a = 0.01$, and by hollow-cylinder analogy based on large-strain theory, assuming $X_o/\delta_1 = 0.15$.
- FIG. 8--Curve for determining location of local minimum in crack-opening stress as a function of the strain-hardening exponent N.
- FIG. 9--Stresses near a blunting crack tip, with transverse plastic strain as a parameter, as calculated by the hollow-cylinder analogy for large strains for N = 0.2 and neglecting elastic strains.

ORNL-DWG 90M-4208 ETD

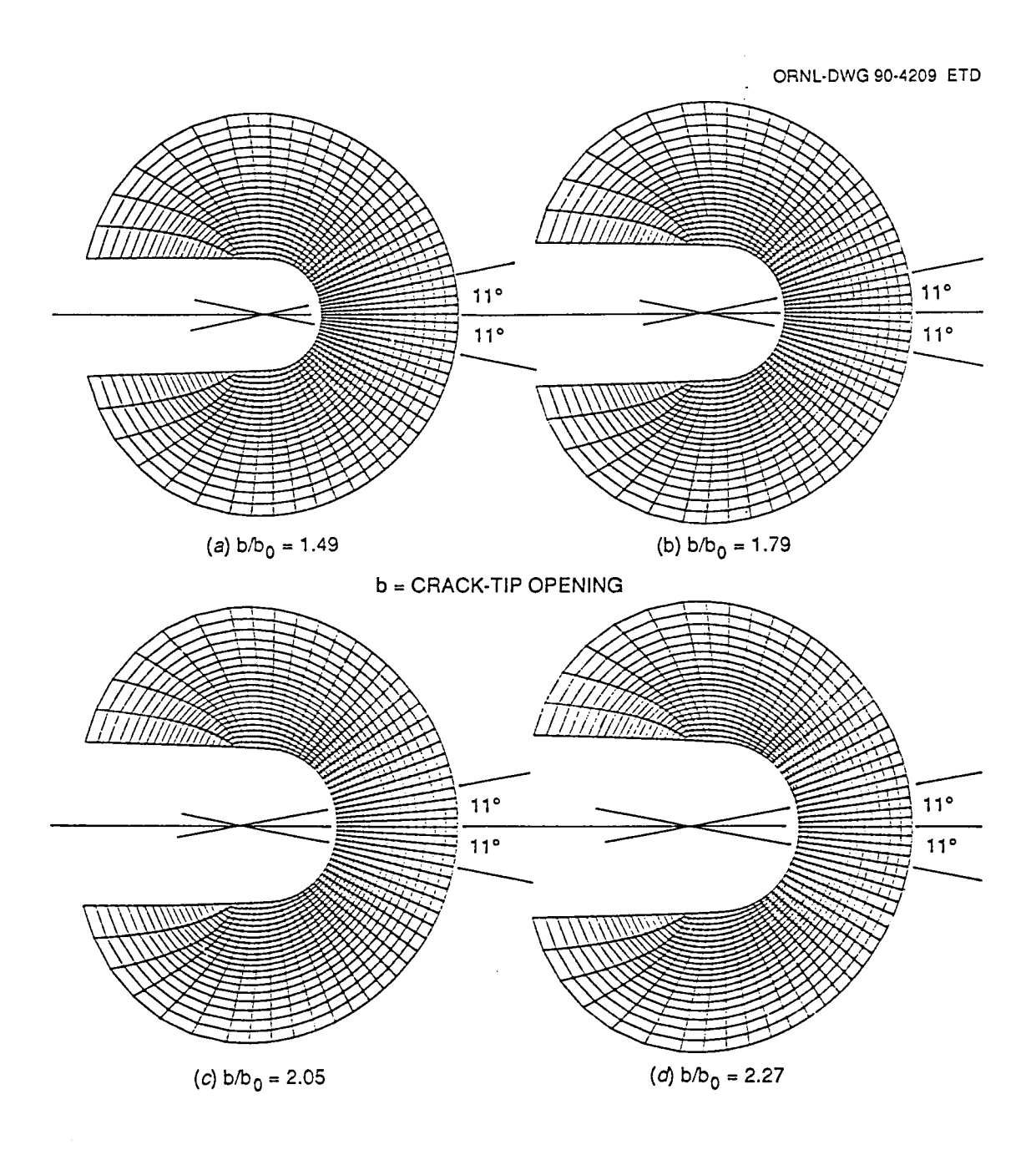


(4) ELASTIC REGION: STRESS AND STRAIN DESCRIBED BY EQUATIONS OF LINEAR-ELASTIC FRACTURE MECHANICS; THIS ZONE CONTROLS STRAINS AND STRESSES IN BOTH PLASTIC ZONES

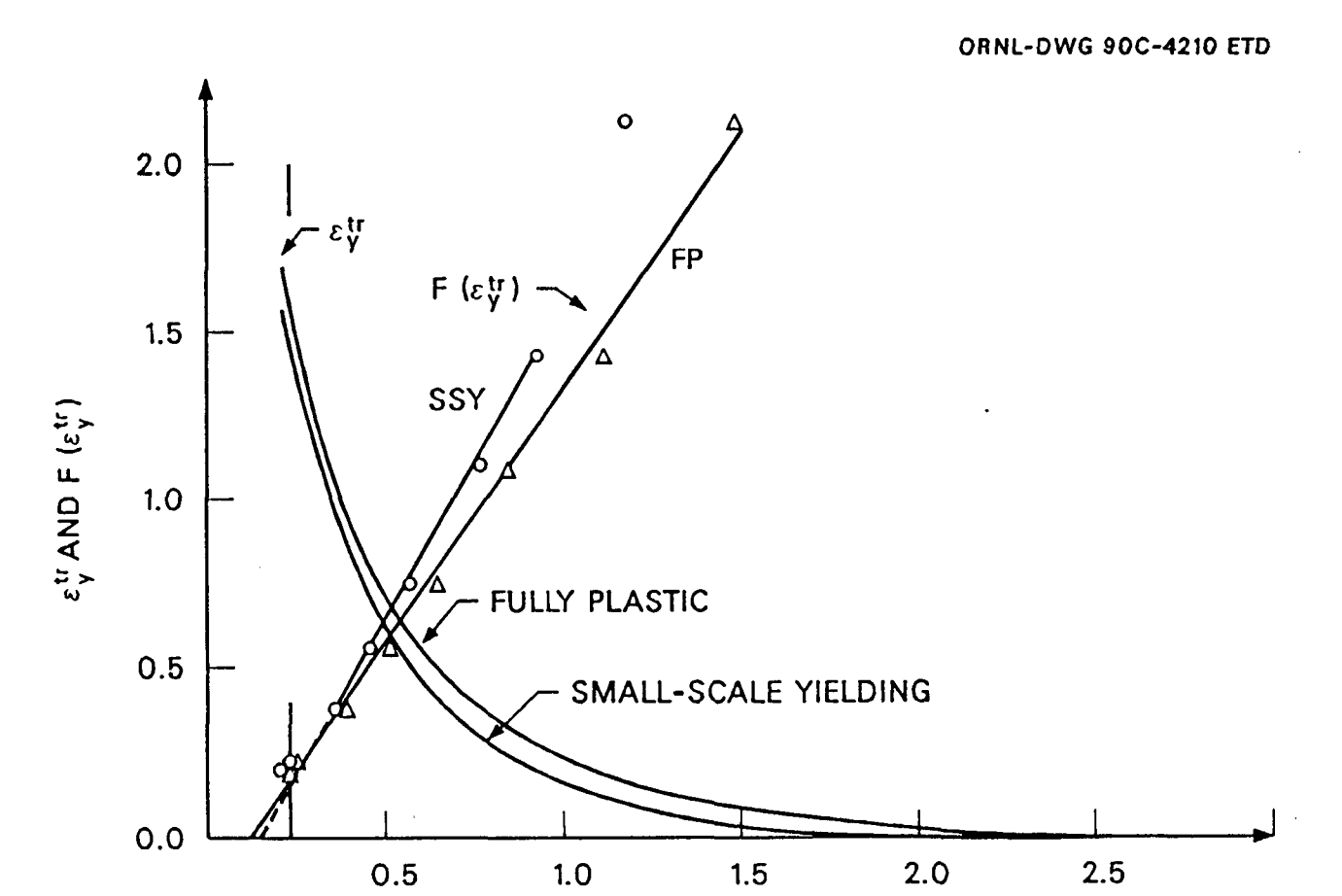
MERKLE FIG. 1



MERKLE FIG. 2



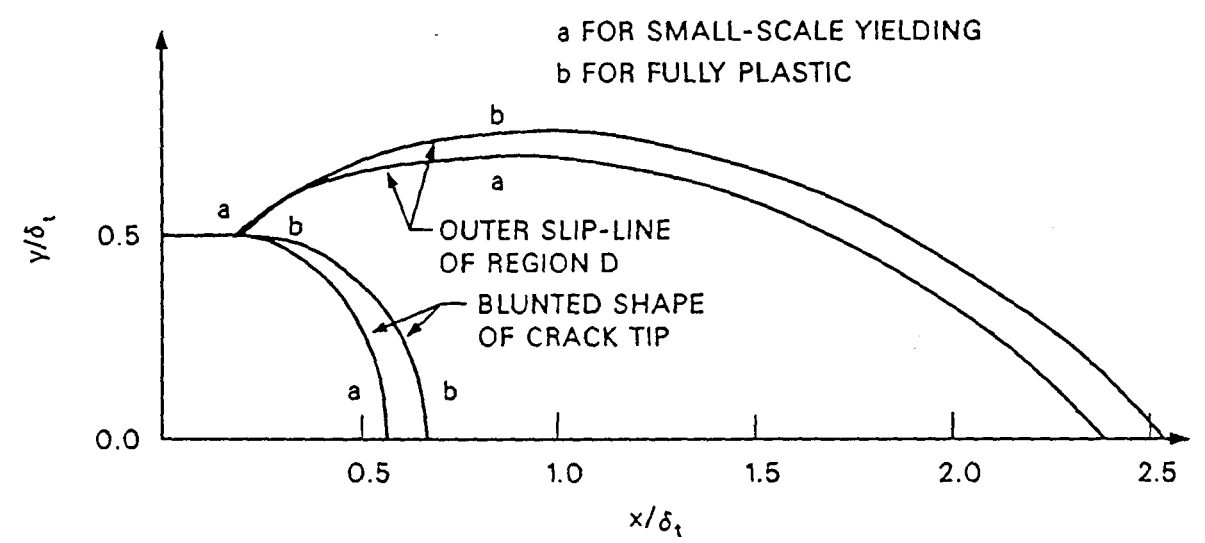
MERKLE FIG. 3



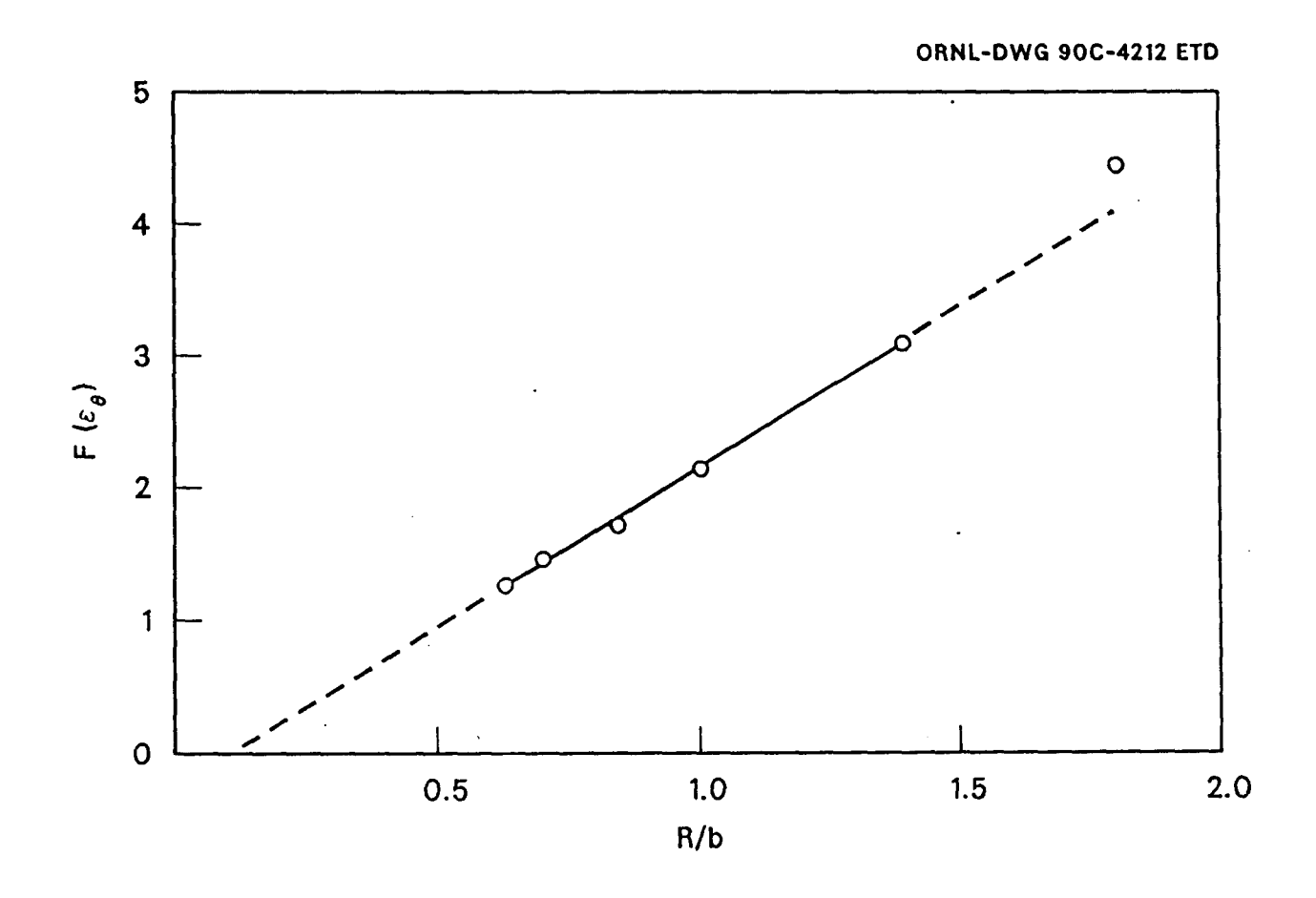
 X/δ_t

MERKLE FIG. 4

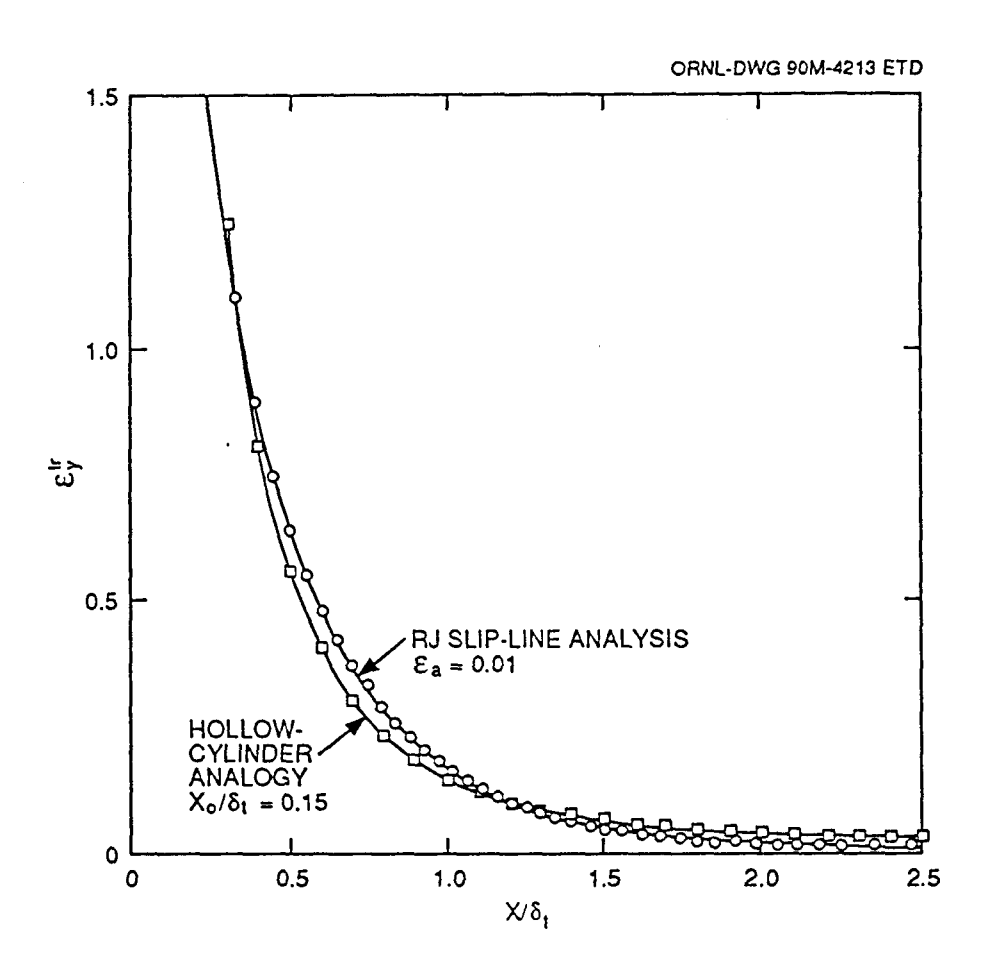




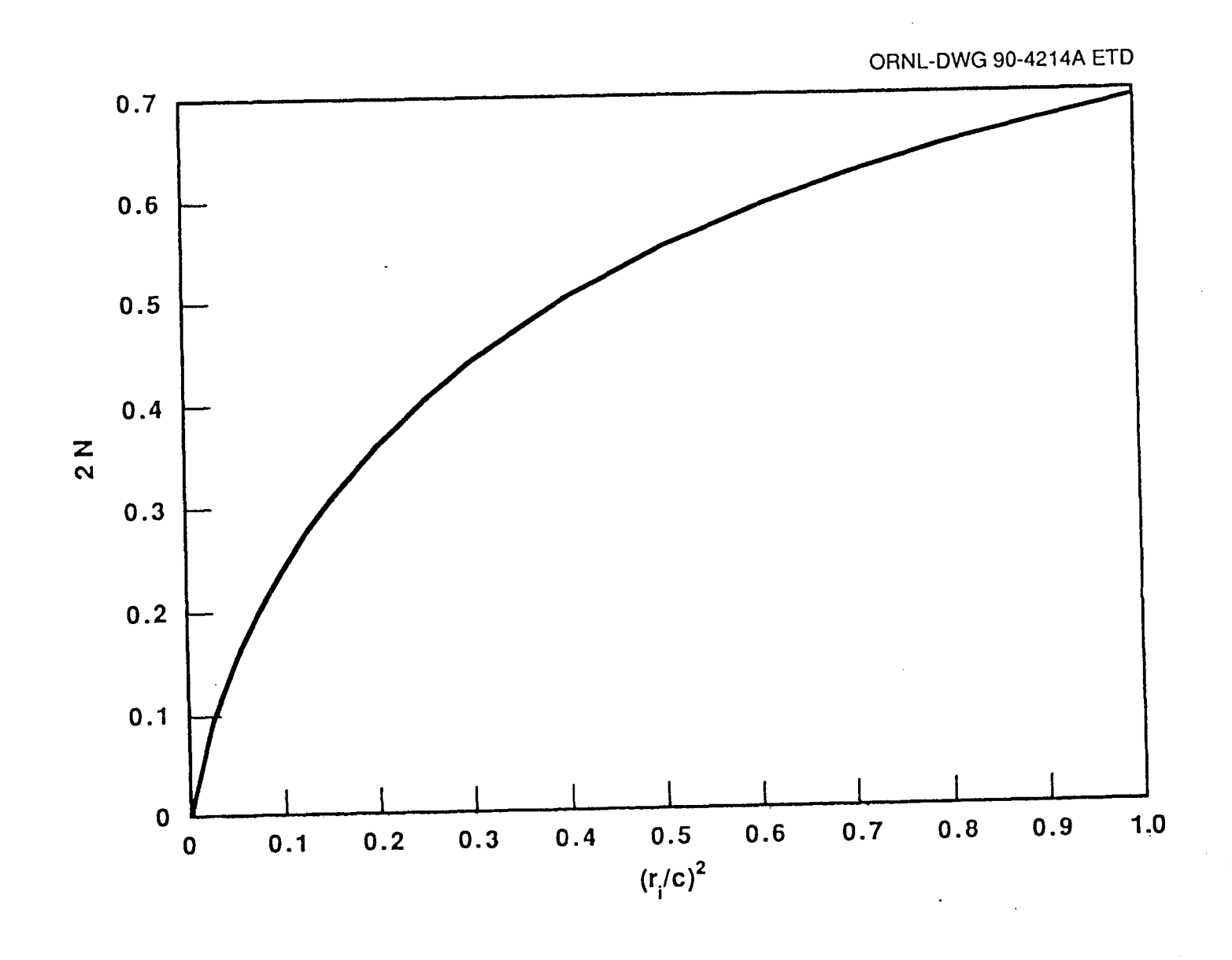
MERKLE FIG. 5



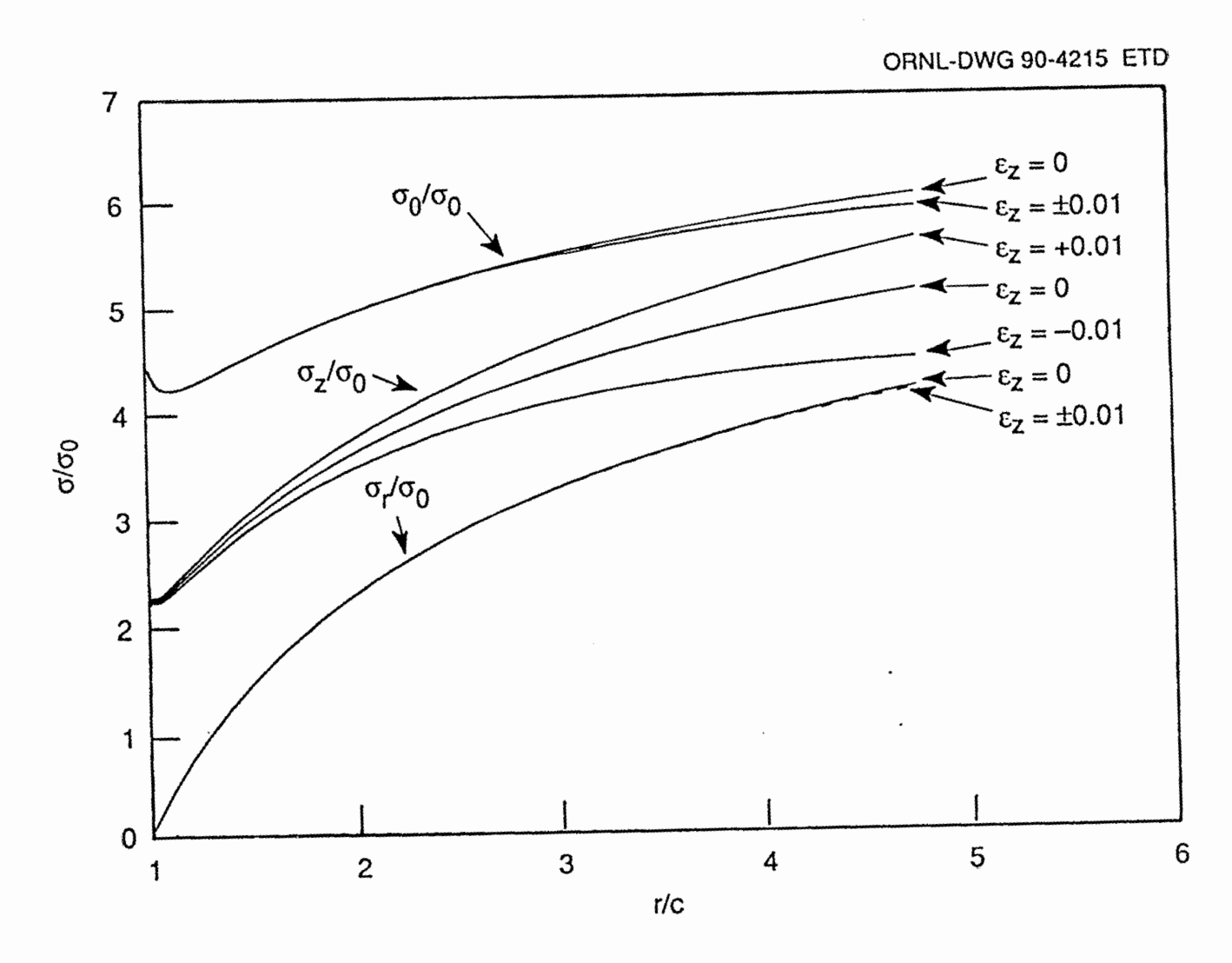
MERKLE FIG. 6



MERKLE FIG. 7



MERKLE FIG. 8



MERKLE FIG. 9